Static Thrust of a Short Primary Linear Reluctance Motor with Simple Secondary Structure

(*)Kokichi Ogawa
(*)Dept. of Mechanical and Energy Systems Engineering, Oita University, Japan
700 Dannoharu, Oita, 870-1192, Japan,
Phone :(+81) 975547799/ Fax: (+81) 975547790, e-mail :ogawa@cc.oita-u.ac.jp

Keywords

Linear synchronous reluctance motor, secondary structure, static thrust

Abstract

A simple secondary structure is strongly demanded in a short primary linear motor. A static test machine of a single-sided linear synchronous reluctance motor with a thin iron reaction plate is manufactured, and the thrust at standstill is measured. Different pitch, width and depth of the iron plates are experimentally estimated, and an example of the available size is considered. Next the static thrust of a double-sided machine is measured and is compared with a single-sided type. 3-D numerical solutions derived from the boundary integral equations are estimated by compared with test results.

1 Introduction

In a short primary linear reluctance motor [1], a reaction plate with simple structure is needed for the saving of construction costs . Authors have examined the performance of a double-sided linear reluctance motor composed of thin iron plates [2]-[4]. The magnetic attractive force in this type does not act in the gravity direction, so that the additional loss between a wheel and a rail is eliminated. However, for a small airgap, it is difficult to maintain a primary member at a magnetic balancing point due to its unstable normal force.

On the other hand, since the attractive force and the weight of a body are supported with a wheel in a single-sided type, the additional loss may increase, but a smaller airgap can be attained easily. It may be applicable to a small capacity use. In this paper, a test machine of a single-sided LRM is manufactured, and the static thrust for different size of thin iron plate is measured. It is shown that a secondary iron plate has typical dimensions of pitch, width and thickness being related to the size of a primary member.

Furthermore, the static thrust of a double-sided machine with the same size of secondary structure is measured and is compared with a single-sided one. 3-D numerical solutions using the boundary integral equations are compared with those test results.

2 Static Test Machine

2.1 Single-sided Test Machine

Fig. 1 shows a 4-pole single-sided test machine. A 3-phase coil is wound around the primary core tooth and it is arranged in two rows. The number of turn of each coil is 160 turns. The coil pitch is 24 mm, where the pole pitch is 36 mm. The total tooth width of two-row arrangement is 34 mm. Each tooth is made of laminated iron with the thickness of 0.5 mm, and has the pitch of 14 mm, the width of 11 mm and the height of 34 mm. A back yoke has the thickness of 6mm. An

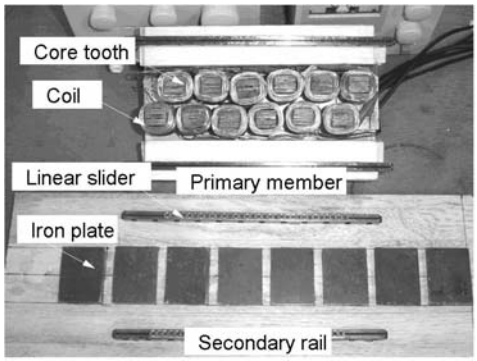

Fig. 1 4-pole single-sided test machine.

example of the secondary iron plate with the pitch of 30 mm, the width of 40 mm and the thickness of 3 mm is periodically arranged along a motor moving direction. In this case the airgap length is adjusted to 1 mm or 2 mm. Linear slider acts as to support and guide the primary member.

2.2 Double-sided Test Machine

A 4-pole double-sided test machine indicated in Fig. 2. A 3-phase coil has the same number of turns as that of a single-sided machine. Each core tooth has the pitch of 14 mm, the height of 13 mm and the width of 36 mm, which is magnetically independent each other. In this machine a back yoke does not exit. The primary member is set in a channel of secondary iron plates. The distance between the walls of the iron plates is 40 mm. The width of core tooth is 36 mm. Then the airgap length on each side of the primary is 2 mm. The linear slider acts as to support and keep the primary member at the symmetrical position. In this case, the magnetic attractive force that works to the primary side is offset.

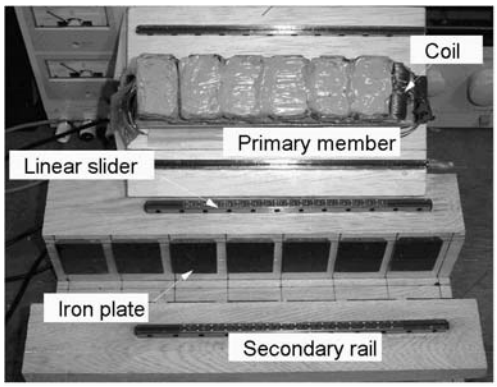

Fig. 2 4-pole double-sided test machine.

A secondary iron plate indicated in Fig.2 has the pitch of 30 mm, the thickness of 3 mm and the width of 40 mm. Its edge in a motor moving direction is tapered by 45 degrees in order to increase the saliency.

3 Test Results for Single-sided Machine

3.1 Effect of Iron width

Fig. 3 shows the load angle characteristic for different width of a secondary plate. The iron pitch is set to 30mm and the thickness is 3mm. The 3-phase AC current with the effective value of 3 A is replaced by the DC current. It corresponds at the time when phase-*a* current takes maximum value of 4.24 A, and phase-*b* and phase–*c* currents take –2.12 A. The distance from the *d*-axis to the phase-*a* coil axis is expressed by the electric angle as a load angle. The airgap length is 1mm.

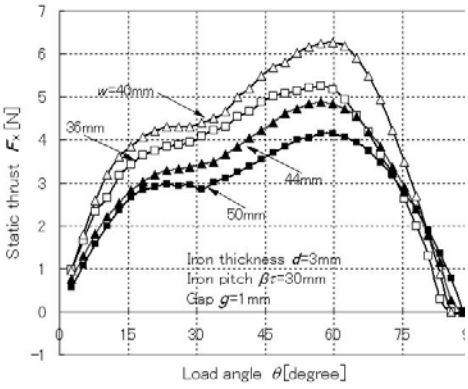

Fig. 3 Static thrust vs load angle characteristics at different secondary iron width.

The static thrust takes the maximum value of 6.27 N at the iron width of 40 mm, which is 6 mm larger than the width of a primary core. As the concentrated coil arrangement is used in this motor, the thrust curve is different from a sinusoidal wave. It means that pulsation of the instantaneous thrust cannot be neglected in this motor.

The peak value of static thrust to the iron width is indicated in Fig. 4. The airgap length is 1 mm and 2 mm. In both cases the static thrust takes the maximum values of 6.27 N (g = 1 mm) and 3.07 N (g = 2 mm) at the iron width of 40 mm. The ratio of the iron width to the total tooth width of the primary is 1.18.

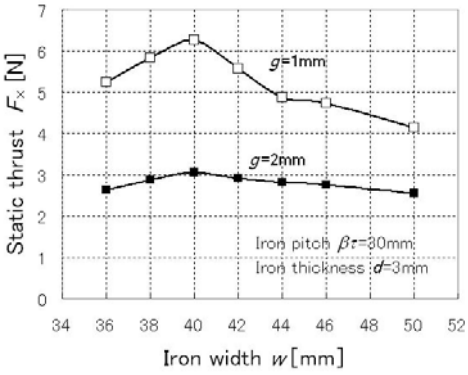

Fig. 4 Maximum .thrust depending on iron width.

3.2 Effect of Iron Pitch

Fig.5 shows load angle characteristics at the iron pitch of 27, 30 and 33mm. As the pole pitch is 36mm, the ratio β to the pole pitch is 0.75, 0.833 and 0.917 respectively. Each curve takes the significantly different form depending on the iron pitch. When the value of β increases, the thrust curve approaches to a sinusoidal wave and the thrust pulsation will reduce. In this case, the maximum value of 6.27 N takes at β = 0.833. This is a typical value for a segmental rotor type [5].

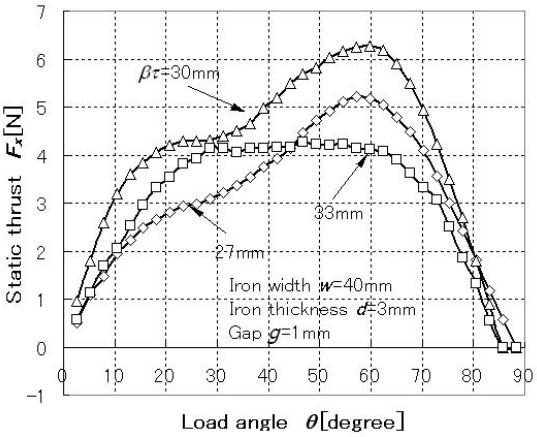

Fig. 5 Static thrust vs load angle characteristics for different iron pitch.

The peak value in load angle characteristics with the different iron pitch is indicated in Fig. 6. It takes the maximum value when the iron pitch is 30mm in both cases of g = 1 mm and 2 mm.

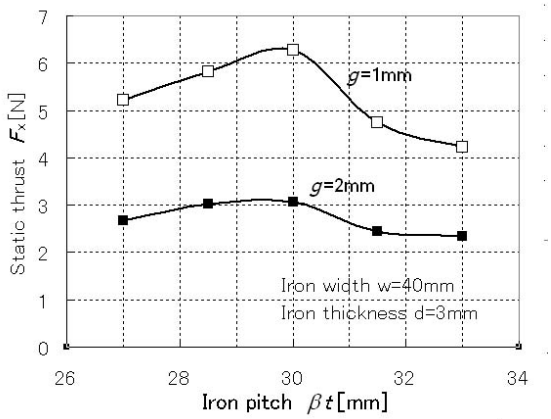

Fig. 6 Maximum thrust depending on iron pitch.

3.3 Effect of Iron Thickness

Fig. 7 shows the static thrust for the different iron thickness. The iron width is set to 40 mm and the iron pitch is 30mm. Since DC current flows in the experiment, the skin effect does not appeared. The static thrust attains the maximum at about 3mm thickness. The thin thickness is desirable to attain the high saliency. When the thickness of iron plate becomes smaller than 3 mm, the thrust reduces due to the magnetic saturation. The reduction is more remarkable at smaller airgap. The thrust at the thickness of 1.5 mm and the air gap of 1mm reduces to 66 % of the thrust at the thickness of 3mm.

3.4 Effect of Airgap Length

The smaller airgap length attains high thrust, where the attractive force also increases. Rigid support mechanism is needed to avoid the contact between the primary and reaction rail. Fig. 8 shows the static thrust for different airgap length at the iron thickness of 3 mm and 6mm. When the airgap length becomes to a half of 2 mm, the static thrust increases to 1.86 times at d = 3 mm and to 1.72 times at d = 6 mm.

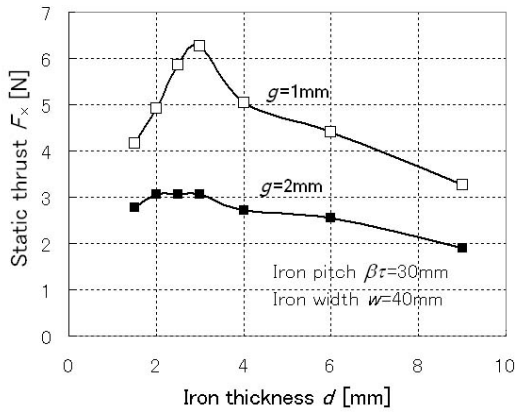

Fig. 7 Maximum thrust depending on iron thickness.

3.5 Effect of Magnitude of Current

The magnetic saturation depends on the magnitude of the primary current. Fig. 9 shows the static thrust depending on the primary current. The horizontal axis is denoted by the effective value.

When the iron thickness is 3 mm and the airgap length is 1mm, the thrust at the current of 3 A is 2.2 times larger than that at 2 A. This ratio is 1.98 times at the airgap length of 2 mm. In this type of motor, the thrust will be proportional to the second power of the primary current when the magnetic

saturation is neglected. The effect of magnetic saturation is small at the iron thickness of 3 mm. When the iron thickness is 1.5 mm, its corresponded value is 1.72 times at the airgap of 1 mm and 1.67 times at airgap of 2 mm. The magnetic saturation is remarkable in this case.

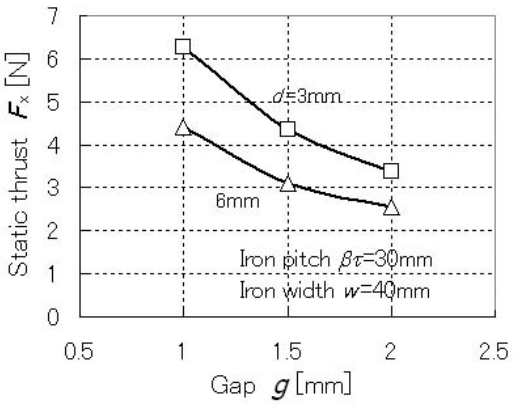

Fig. 8 Maximum thrust depending on airgap length.

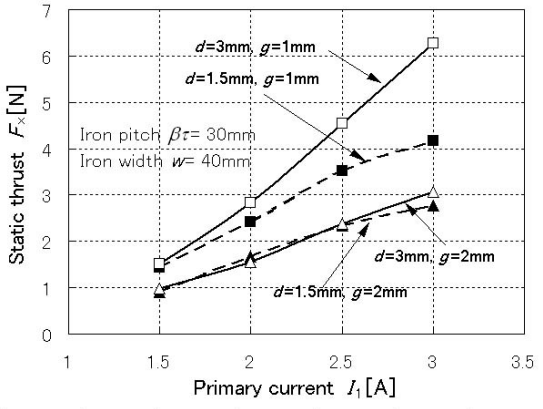

Fig. 9 Maximum thrust depending on primary current.

3.6 Effect of Edge Tapering

The authors proposed that iron plate with tapered edge is effective by using the 3-D numerical calculation as described in [2]-[4]. In the analysis, the magnetic saturation is not considered. In this section the edge tapering is experimentally estimated. Fig. 10 shows the load angle characteristics for an iron plate with or without edge tapering. Both iron plates have the width of 40 mm, the pitch of 30 mm and the thickness of 3 mm. The tapering angle is 45 degrees, where the inner iron pitch facing to the primary pole face is 30 mm and the outer pitch is 24 mm. The iron plate with tapered edge is a little bit lower than that without tapered edge. It is recognized that the edge tapering not available when the thickness of iron plate is relatively thin because of magnetic saturation.

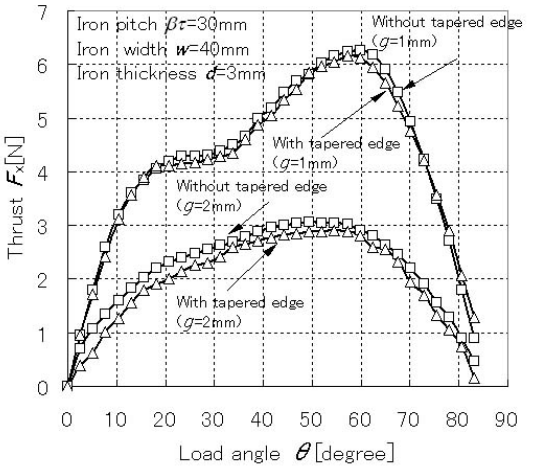

Fig. 10 Load angle characteristics with or without tapered edge.

.

4 Analysis and Test Results for double-sided Machine

4.1 3-D Analysis

A model used for numerical calculation is shown in Fig. 11. A 3-phase coil is wound around the primary core and is arranged in two lrows. The number of turn of each coil is 160 turns and 3-phase current of 3A flows in it.

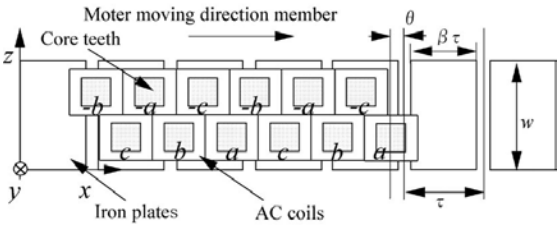

Fig. 11 Model for numerical calculation.

The boundary integral equation used for 3-D numerical analysis [6] is shown in (1):

$$\{1+(1/\chi)\}\boldsymbol{k}(\boldsymbol{r}) = \int_{\Gamma} \boldsymbol{k}(\boldsymbol{r}') \times \frac{(\boldsymbol{r}-\boldsymbol{r}')}{4\pi|\boldsymbol{r}-\boldsymbol{r}'|^3} \times \boldsymbol{n}(\boldsymbol{r}) d\Gamma' + \int_{\Omega} \boldsymbol{j}_0(\boldsymbol{r}') \times \frac{(\boldsymbol{r}-\boldsymbol{r}')}{4\pi|\boldsymbol{r}-\boldsymbol{r}'|^3} \times \boldsymbol{n}(\boldsymbol{r}) d\Omega' \quad (1)$$

where

$$\chi = \mu_r - 1 \quad (2)$$

The symbol $\boldsymbol{k}(\boldsymbol{r}')$ is the surface magnetizing current of a secondary iron plate and a primary core tooth. The symbol $\boldsymbol{j}_0(\boldsymbol{r}')$ is 3-phase alternating current. The symbol $\boldsymbol{n}(\boldsymbol{r})$ denotes the outward normal vector on a secondary iron surface or a primary core tooth surface. The relative permeability μ_r of ferromagnetic material is assumed to be 5000. The eddy current in an iron plate is neglected.

Electromagnetic force $\boldsymbol{F}$ is derived by the numerical integration of the product of the current density and the flux densityin a 3-phase coil region Ω and on the surface of a primary core tooth Γ_1.

$$\boldsymbol{F} = \int_{\Gamma_1} \boldsymbol{k}(\boldsymbol{r}) \times \left\{ \int_{\Gamma_2} \mu_0 \boldsymbol{k}_2(\boldsymbol{r}') \times \frac{(\boldsymbol{r}-\boldsymbol{r}')}{4\pi|\boldsymbol{r}-\boldsymbol{r}'|^3} d\Gamma' \right\} d\Gamma + \int_{\Omega} \boldsymbol{J}_0(\boldsymbol{r}) \times \left\{ \int_{\Gamma_2} \mu_0 \boldsymbol{k}_2(\boldsymbol{r}') \times \frac{(\boldsymbol{r}-\boldsymbol{r}')}{4\pi|\boldsymbol{r}-\boldsymbol{r}'|^3} d\Gamma' \right\} d\Omega \quad (3)$$

The symbol $\boldsymbol{k}_2(\boldsymbol{r}')$ is surface magnetizing current in secondary iron plate of the region Γ_2.

Mesh division of a 4-pole LRM is shown in Fig. 12. The geometrical symmetry is used so that mesh division is performed in a half region. Triangle elements are applied to the region of the surface magnetizing current, and triangular prism elements are used for the region where the 3-phase alternating current flows.

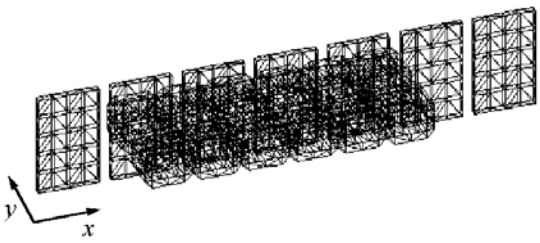

Fig. 12. Mesh division of 4-pole double-sided LRM.

4.2 Test Results and Calculated Results

Fig.13 shows test results and calculated results for double-sided machines. Iron plates used here have the same dimensions as those used in single-sided machines. In the figure, the measured value corresponds to the instantaneous thrust at the time when the phase-a current becomes maximum. The calculated result corresponds to the averaged thrust.

In the single-sided machine, the static thrust of iron plate with tapered edge is a little bit lower than that without tapered edge as discussed in section 3.5. On the other hand, for this double-sided machine, the peak value with tapered edge is by 3.1 % greater than that without tapered edge.

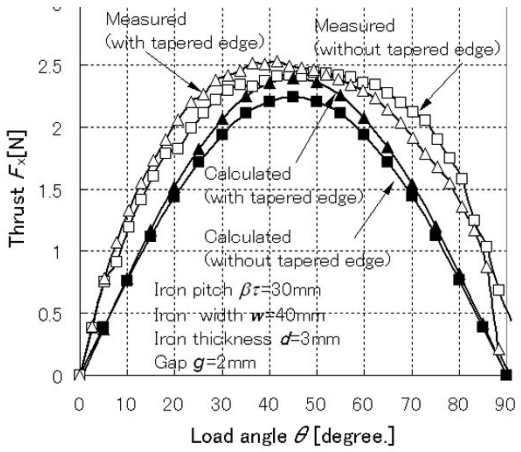

Fig. 13 Load angle characteristics in 4-pole double-sided test machine.

The static thrust for a single-sided machine without tapered edge is by 26 % greater than that for a double-sided machine. For the iron plate with tapered edge, it is by 12 % greater than the double-sided type.

Next Test results for double-sided machines are compared with calculated results. Test result is by 4.9 % greater than the calculated one for the iron plate without tapered edge. It is by 8.6 % greater that for the iron plate with tapered edge.

Fig. 14 shows the instantaneous thrust for the iron plates with or without tapered edge, which is given by 3-D calculation. The concentrated coil arrangement is used in this test machine. The amplitude of the thrust pulsation with the tapered edge is 15.8 % of the average thrust of 2.36 N. That without tapered edge is 16 % of the average thrust of 2.22 N. The thrust pulsation will not be ignored.

5 Conclusion

The static thrust of a single-sided linear reluctance motor was examined for different secondary size. Examples of the typical values of the iron pitch, width and thickness are founded. It is recognized that the ratio of the iron pitch to the pole pitch has a typical value of 0.833 for a segmental rotor type [5]. The desirable iron width is a little bit greater than the primary core width. A thin iron plate is preferable, but it must be decided by considering the magnetic saturation.

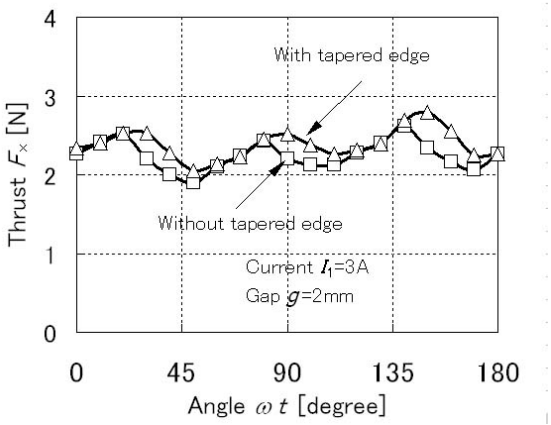

Fig. 14 Instantaneous waveforms of thrust at load angle 45 degrees.

Next the single-sided and the double-sided machines are compared by using the same secondary plates. The static thrust of the single-sided type is by 10 to 20 % greater than the double-sided type.

Calculated results for the double-sided machine are compared with test results. Test results are several percent greater than 3-D calculation results.

References

1. I. Boldia, S.A. Nasar. *Thrust and normal forces in a segmented-secondary linear reluctance motor,* Proc. IEE, Vol.122, No.9, pp.922-924, September 1975
2. K. Ogawa. *Performance of a Linear Reluctance Motor with Novel Structure,* International Symposium on Linear Drives for Industry Applications (LDIA2003), pp.57-60, September 2003.
3. K. Ogawa, T. Matsuo. *A New Construction of a Short Primary Linear Reluctance Motor,* 6th Japan-France Congress on Mechatronics and 4th Asia-Europe Congress on Mechatronics, pp.535-540, September 2003.
4. K. Ogawa. *Secondary Geometry of a Short Primary Linear Reluctance Motor,* The 2nd International Conference on Mechatronics and Information Technology (ICMIT 2003), pp.474-479, December 2003.
5. J. D. Edwards, A. M. El-Antably. *Segmental-rotor linear reluctance motors with large airgaps,* Proc. IEE, Vol. 125, No.1, pp.210-215, March 1978.
6. T. Morisue. *Gauge computational electromagnetism and gauges,* Morikita Shuppan, 1996.